Journal of Power Sources 266 (2014) 29–35

Contents lists available at ScienceDirect

Journal of Power Sources

journal homepage: www.elsevier.com/locate/jpowsour

A novel hierarchically structured and highly hydrophilic poly(vinyl alcohol-*co*-ethylene)/poly(ethylene terephthalate) nanoporous membrane for lithium-ion battery separator

Ming Xia, Qiongzhen Liu, Zhou Zhou, Yifei Tao, MuFang Li, Ke Liu, Zhihong Wu, Dong Wang*

College of Materials Science and Engineering, Wuhan Textile University, Wuhan 430200, China

HIGHLIGHTS

- Novel nonwoven based nanoporous separators for use in lithium batteries.
- A facile way to tune nanoporous structure for nonwoven based separators.
- PET nonwoven sandwiched between nanofibrous membranes forms hierarchical structure.
- PVA-*co*-PE nanofibers allow good wettability for the nonwoven based separators.
- This structural novelty allows high porosity and lower thermal shrinkage.

ARTICLE INFO

Article history:
Received 27 January 2014
Received in revised form
4 April 2014
Accepted 30 April 2014
Available online 14 May 2014

Keywords:
Lithium-ion batteries
Nanofibrous separator
Hierarchically nanoporous structure
Wettability
Ion conductivity

ABSTRACT

A novel hierarchically structured and highly hydrophilic poly(vinyl alcohol-*co*-ethylene)/poly(ethylene terephthalate) nanoporous separator (referred to NFs/PET/NFs) composed of a poly(ethylene terephthalate) (PET) nonwoven sandwiched between two interconnected poly(vinyl alcohol-*co*-ethylene) (PVA-*co*-PE) nanofibrous membranes is successfully developed for lithium-ion battery. Systematical investigations including structural characterization, porosity measurement, water contact angle testing, electrolyte uptake, and thermal shrinkage testing demonstrate that the notable feature of this NFs/PET/NFs nanofibrous separator is an electrolyte-philic, highly porous and hierarchically nanoscaled structure, thus resulting in superior electrolyte wettability, lower thermal shrinkage, and higher ion conductivity, in comparison to the commercial Polypropylene (PP) separator. These structural characteristics enable the NFs/PET/NFs separator to offer an excellent cell performance including outstanding C-rate capability, high capacity and excellent cycling performance. This suggests that the NFs/PET/NFs separator is a promising material for practical application in lithium-ion battery due to it low cost production and high performance.

1. Introduction

With fast development of portable electronics devices such as smart mobiles (iPhone, iPad and so on) and emerging fields in new energy vehicles, lithium-ion batteries have recently attracted increasing attention, due to their renewable and clear energy as well as high open circuit voltage, high energy density and long cycling life [1–5]. The separator is known as a critical functional component of lithium-ion battery. Specifically, the important function of the separator is to ensure the isolation of cathode and anode in the battery, and to provide a well-designed porous structure for lithium-ion transport [6–9].

At present, commercial polyolefin-based membranes such as PP, PE and PP/PE/PP have been widely used as the separator of lithium-ion battery, owing to their chemical stability, and uniformity in pore size distribution. However, their inferior thermal stability may cause serious security issues. Additionally, their low porosity and insufficient electrolyte wettability will restrict the ionic transport [10]. Polyolefin nonwovens-based membranes have drawn considerable attention as a promising separator for lithium-ion

* Corresponding author. Tel.: +86 27 59367691.
E-mail address: wangdon08@126.com (D. Wang).

http://dx.doi.org/10.1016/j.jpowsour.2014.04.151
0378-7753/

batteries, as their low cost, excellent thermal resistant and high porosity. However, the conventional nonwovens cannot be directly applicable as a separator, resulting from their native macroscaled porosity and nonuniform pore size distribution [11]. Considerable efforts have been paid to overcome the drawbacks of nonwovens, including coating of selective nanopowders onto nonwoven substrate, coating of electro-spinning nanofibers, and so on. Though electro-spinning nanofibers can provide well-tuned structure applicable as a separator, the big issue is that their low production efficiency, which restricts the large-scale production in factory.

In the present study, we demonstrate a facile way to construct a three-dimensional well-tuned hierarchical structure comprising a macroscaled poly(ethylene terephthalate) (PET) nonwoven sandwiched between two nanoscaled porous poly(vinyl alcohol-*co*-ethylene) (PVA-*co*-PE) nanofibrous membranes (referred to as a NFs/PET/NFs separator). This hierarchically structured NFs/PET/NFs separator also offers high hydrophilicity due to the high water affinity and large specific area of the PVA-*co*-PE nanofibers [12]. To evaluate the cell performance of the NFs/PET/NFs separator, a commercialized PP separator was also investigated for comparison in this study. The microstructure of porous structure, porosity, thermal shrinkage, electrolyte wettability, and ion conductivity were carried out to characterize the structural superiorities of our NFs/PET/NFs separator. Finally, the effect of NFs/PET/NFs separator on the cell performance including discharge capacities, discharge C-rate capability, and cycle performance were also investigated.

2. Experimental

2.1. Material

Poly(ethylene terephthalate) (PVA-*co*-PE) (ethylene content is 44 mol %) was purchased from Sigma–Aldrich (Milwaukee, WI). Cellulose acetate butyrate (CAB, buttery content 35–39%) was purchased from the Eastman Chemical (Kingsport, TN). Isopropyl alcohol, acetone, 1-methyl-2-pyrrolidinone (NMP) were from Sinopharm Chemical Reagent Co., Ltd. Acetylene black, PVDF powder and $LiFePO_4$ powder ware purchased from Shenzhen PengXiang YunDa Machinery Co., Ltd. A Spun-bond poly(ethylene terephthalate) (PET) nonwoven substrate (10 g m^{-2}) with thickness of 36 μm was purchased from Shandong Taipeng Nonwoven Co., Ltd. A commercial PP separator with the thickness of 25 μm is also purchased from Celgard China for comparison with our separator.

2.2. Fabrication of NFs/PET/NFs separator

PVA-*co*-PE nanofibers were prepared according to previous methods reported in literature [13]. The mixture PVA-*co*-PE/CAB (w/w = 20/80) was fed into a Leistritz corotating twin-screw (18 mm) extruder (Model MIC 18/GL 30D, Nurnberg, Germany) at a feed rate of 12 g min^{-1}. Twin-screw extruder processing temperature parameters ranged from 190 to 230 °C. The blends were extruded with a draw ratio of 25 (the area of cross section of the die to that of the extrudates) and cooled by water. The PVA-*co*-PE nanofibers in form of continuous yarns were prepared by the extraction of CAB matrix. The typical procedure was that PVA-*co*-PE nanofibers were dispersed in an aqueous solution with a high speed shear mixer to form a stable suspension. The suspension was then coated onto the washed surface of the PET nonwoven substrates with a casting knife to form nanofibers NFs/PET/NFs membranes. The schematic diagram of preparation of NFs/PET/NFs separator and lithium-ion transport through the separator is shown in Scheme 1. It is seen that the macro-sized porous PET nonwoven (36 μm) is sandwiched between two PAV-*co*-PE nanofibrous membrane (4 μm in thickness for one side). The total thickness of NFs/PET/NFs separator in present study is about 44 μm.

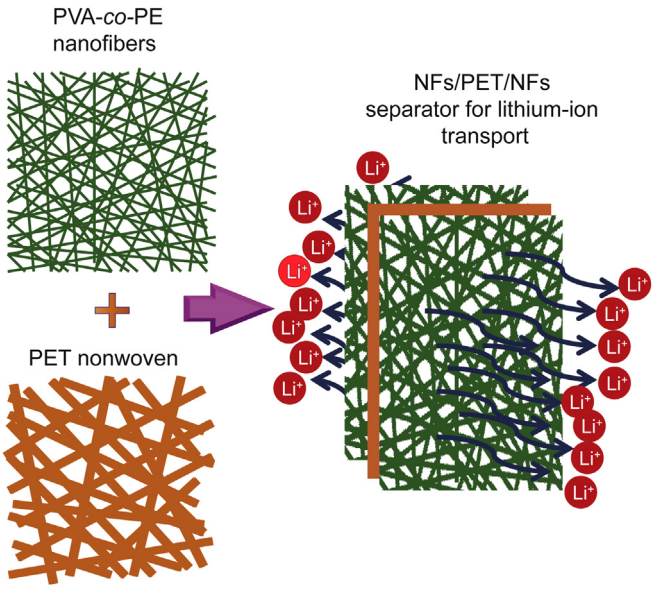

Scheme 1. The schematic representation of the NFs/PET/NFs separator made of PET nonwoven sandwiched by PVA-*co*-PE nanofibers layers and lithium-ion transport through the separator.

2.3. Characterization

The porous structure and the morphology of the fibers of the separators were investigated by a Scanning Electron Microscopy (SEM) (JEOL, JSM-6510L). The thermal shrinkage of the separators was determined by measuring the dimensional change (area based) before and after heat treatment at 150 °C for 30 min.

The porosity was calculated using Equation (1)

$$\text{Porosity}\ (\%) = \left(W_{\text{wet}} - W_{\text{dry}}\right)/\left(\rho_b \times V_{\text{dry}}\right), \quad (1)$$

where W_{dry} and W_{wet} represent the weights of the separator before and after immersion in *n*-butanol for 1 h, ρ_b is the density of *n*-butanol, and V_{dry} is the apparent volume of the separator.

The wettability was measured with a water droplet on a separator and recorded by a contact angle analyzer (FM40 Easy Drop, KRUSS). The electrolyte uptake was measured using the following Equation (2)

$$\text{Electrolyte uptake}\ (\%) = (W_2 - W_1)/W_1 \times 100, \quad (2)$$

where W_1 and W_2 represents the weights of the separators before and after soaking them in a liquid electrolyte (1 M $LiPF_6$ in Ethylene carbonate (EC)–Dimethyl carbonate (DMC) (50/50, vol/vol) for 1 h.

The electrochemical stability window of the separators was measured by the linear sweep voltammetry (LSV) using an Autolab system (PGSTAT302, Switzerland). A liquid-electrolyte soaked separator was sandwiched with stainless steel as a working electrode and lithium-metal as a counter and reference electrode. The LSV test for the separators was carried out over a voltage range 3.6–6.0 V vs. Li^+/Li at a scan rate of 1.0 mV s^{-1}.

The ion conductivity of the separators was obtained by electrochemical impedance spectroscopy (EIS, PGSTAT302, Autolab) at amplitude of 5 mV over a frequency range of 0.01–10^4 Hz. The separators soaked in liquid-electrolyte was sandwiching between

two stainless steel electrodes. The ion conductivity was calculated by Equation (3)

$$\sigma = d/(R_b \times S), \quad (3)$$

where σ is ion conductivity of the separator, d is the thickness of the separator, R_b is the bulk resistance, and S is the area of the separator. The area of all the separators was 2.54 cm^2.

A unit cell (CR2016-type coin) was assembled by sandwiching the separator between a $LiFePO_4$ cathode ($LiFePO_4$/Acetylene black/PVDF = 80/10/10, wt/wt/wt) and a Lithium metal anode wetted by a liquid electrolyte (1 M $LiPF_6$ in EC/DMC (1/1, v/v)) conducted in an argon-filled glove box (GP20, Etelux). The charge/discharge capacities, C-rate discharge capability, and cycling performance of cells were evaluated using a LAND battery test system (CT 2001A). The discharge current densities vary from 0.2 C (1 C = 170 mAh g^{-1}) to 2.0 C at a constant charge current density of 0.2 C under a voltage range of 2.5–4.3 V. To evaluate the cycling performance, the cells were measured at a constant charge/discharge of 0.5 C/0.5 C for 100 cycles. Specific capacities of the cells were calculated based on the weight of active material ($LiFePO_4$) in the cathode.

3. Results and discussion

3.1. Morphology and structure

The porous structures of the separators are examined by SEM observations. The typical morphology of the commercial PP separator is presented in Fig. 1(a) and (b), indicating needle-like nano-scaled pores distributed along the dry-stretching direction. The pore size is apparent is anisotropic with one dimension is about 500 nm and another dimension is about 20 nm. It is seemingly that the porosity of the separator is not very high, thus restricting the ion transport. Fig. 1(c) shows that the native PET nonwoven is consisted of randomly intertwined fibers forming macro-sized pores with the size ranging from 50 to 100 μm. The porosity of the PET nonwoven is measured to be about 78%. This excessively large-sized porous structure is obviously unfavorable for separator, as it will cause self-discharge and uneven current distribution [14]. To overcome the structural drawbacks of the PET nonwoven, a hierarchically structured NFs/PET/NFs separator is constructed by the macro-scaled PET nonwoven sandwiched between two PVA-*co*-PE nanofibrous membrane as shown in Fig. 1(e), where the morphology of the PVA-*co*-PE nanofibers with the diameter about

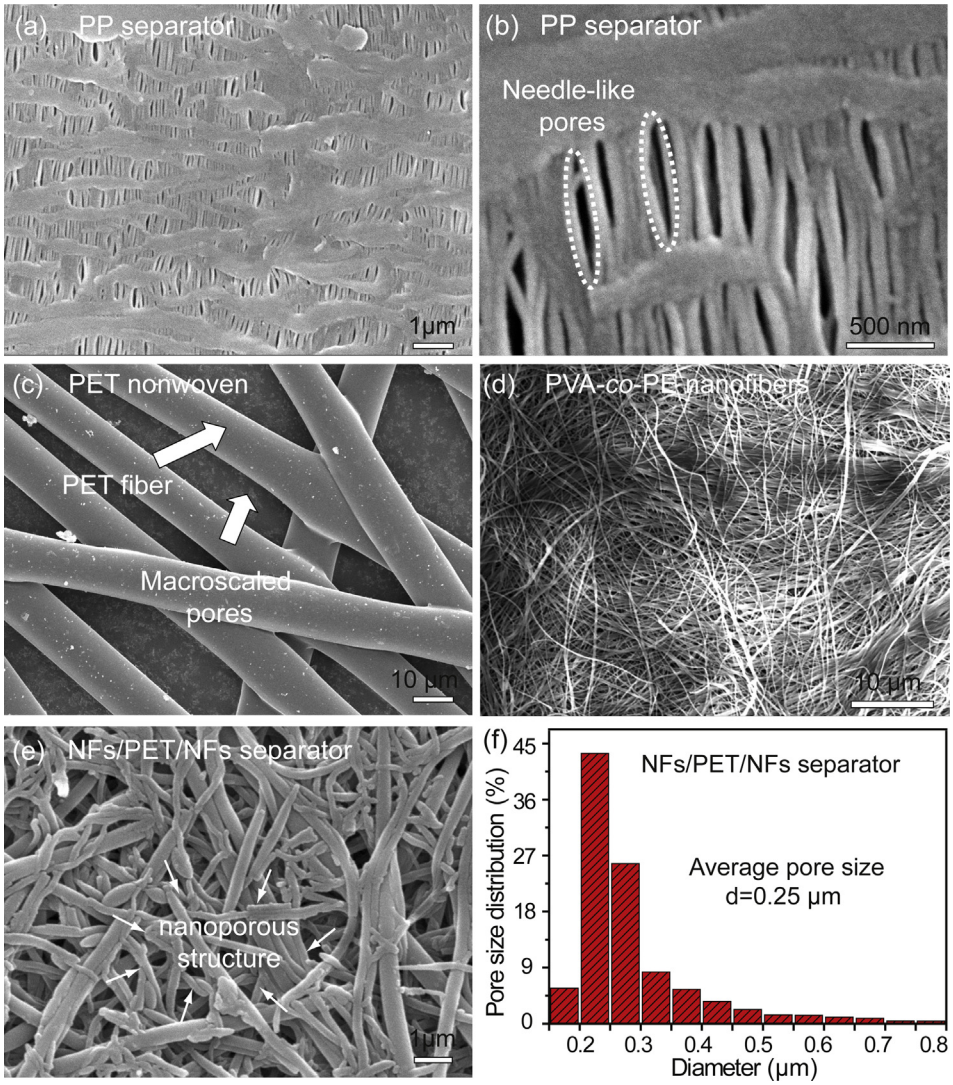

Fig. 1. SEM morphologies of (a–b) commercial PP separator (low and high magnification), (c) 10 g m^{-2} spun-bond PET nonwoven, (d) PVA-*co*-PE nanofibers, (e) NFs/PET/NFs separator and (f) its pore size distribution.

100–300 nm is presented in Fig. 1(d). The macro-sized pores in the PET nonwoven are homogenously covered with the top and down-layered PVA-*co*-PE nanofibrous membrane. The average diameter of the composite NFs/PET/NFs separator is well tuned to be 250 nm according to the pore size distribution presented in Fig. 1(f). Therefore, this hierarchically structured separator offers three-dimensional interconnected nanoscaled porous structure and high porosity, thus facilitating lithium ion transport and ensuring electrolyte affinity.

Porosity is one of the key parameters that affect ion conductivity of the separator infiltrated with the electrolyte. It will greatly affect battery charge and discharge performance [15]. The porosity of the NFs/PET/NFs separator is evaluated to be about 54.2%, which is much higher than that of the commercial PP separator (37%) according to aforementioned Equation (1). This result agrees well with the SEM observations, indicating that the porosity of this hierarchically structured NFs/PET/NFs separator is fairly high.

3.2. The wettability and electrolyte uptake of separator

The wettability of the separators is evaluated by water contact angle test, and the results are shown in Fig. 2. It is impressed from Fig. 2(c) that the NFs/PET/NFs separator is quickly wetted by water, showing good hydrophilicity and high surface energy, while PP and native PET nonwoven separator are hardly wetted by water. The calculated water angle of NFs/PET/NFs separator is 57.5°, which is much lower than that of commercial PP (118.4°), and that of native PET nonwoven separator (113.2°). The electrolyte uptake of the NFs/PET/NFs separator (159.7%) is slightly larger than that of the commercial PP separator (~141.2%), demonstrating that the NFs/PET/NFs separator is promising alternative to commercial PP separator for lithium-ion battery. Also, the result of electrolyte uptake is well accordance with the water contact angle testing.

The NFs/PET/NFs separator presents superior electrolyte wettability than that of commercial PP and nonwoven PET separator, ascribing to its hierarchically interconnected three-dimensional nano-porous structure and high hydrophilicity of PVA-*co*-PE nanofibers who possessing abundant functional hydroxyl groups [13]. It is known that the wettability of separator greatly affects lithium-ion battery performance [16]. Considering the excellent electrolyte wettability, the NFs/PET/NFs separator is expected to provide higher ion conductivity and better cell performance of the lithium-ion batteries.

3.3. Thermal property

The thermal shrinkage of separators is closely related to the safety performance of lithium-ion battery [17,18]. Fig. 3 shows that the dimensional change of NFs/PET/NFs separator almost can be negligible at 150 °C, while the PP separator shows significant shrinkage as high as 33%. This indicates that the hierarchical structure of the NFs/PET/NFs separator is more thermally stable than that of the commercial PP separator. The poor thermal shrinkage of the commercial PP separator is originating from stretching processes during its fabrication in order to form the nanosized pores [6,8]. In comparison, the NFs/PET/NFs separator is

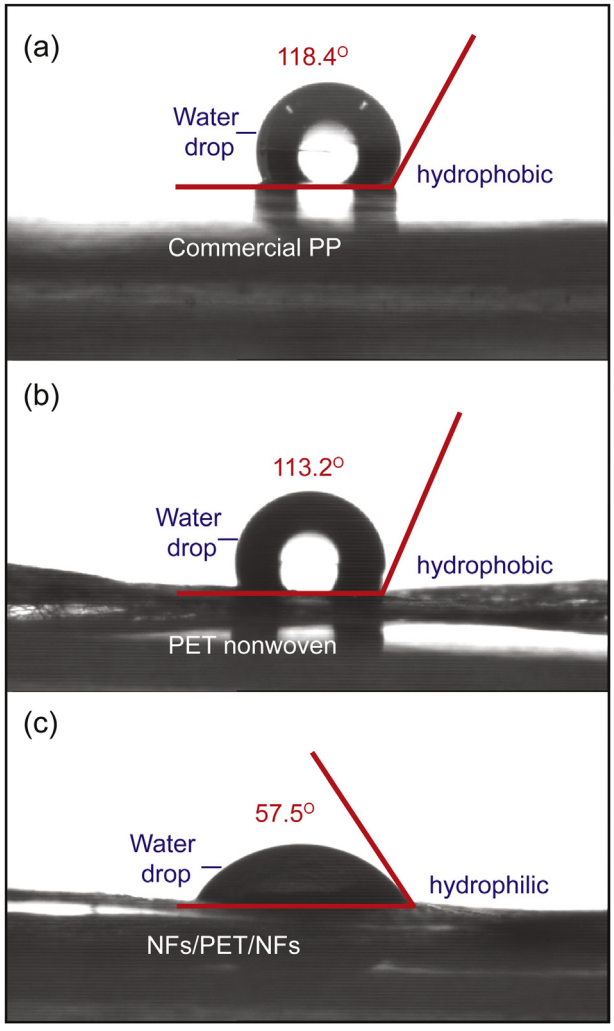

Fig. 2. Photographs of static water contact angle of (a) PP separator, (b) 10 g m^{-2} spunbond PET nonwoven and (c) NFs/PET/NFs separator.

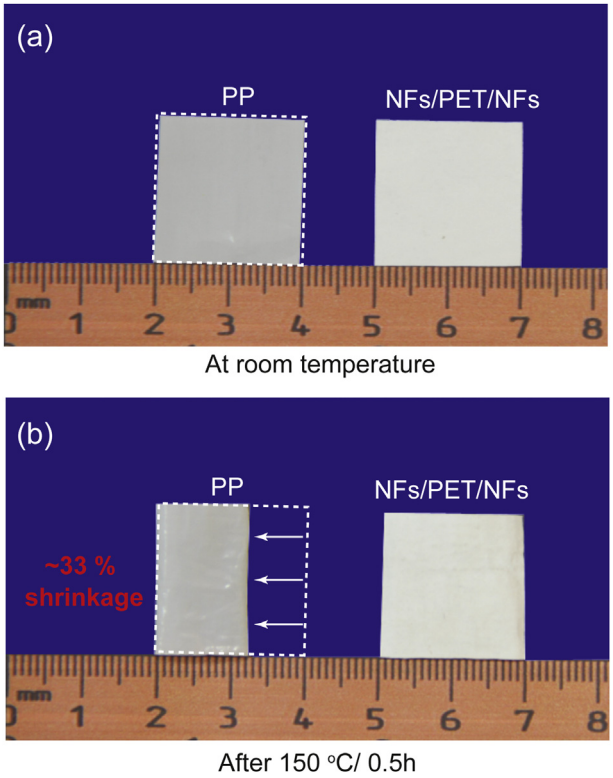

Fig. 3. Photographs showing thermal shrinkage of the separators (a) before and (b) after heat treatment.

not subjected to such kind distortion process, thus retain the intrinsic high mechanical (average tensile strength about 35 N/5 cm) and thermal stability of the PET nonwoven (thermal shrinkage $\leq$ 2.5%) and the interconnected nanoscaled porous structure of PVA-*co*-PE nanofibrous membrane.

3.4. The electrochemical properties of separator

The electrochemical stability window of the NFs/PET/NFs separator is evaluated by a linear sweep voltammetry experiment as shown in Fig. 4. It is clearly seen that there is no anodic currents are observed below 4.7 V vs. Li^+/Li for the NFs/PET/NFs separator, which is comparable to that of the commercial PP separator. It is noticed that the decomposition voltage of the electrode in this study for all the separators is no more than 4.7 V. These results suggest that the NFs/PET/NFs separator can be applicable to a lithium-ion battery [19,20].

Fig. 5 shows the Nyquist curves of the liquid electrolyte-soaked separators. The straight lines inclined towards the Z' axis represents the electrode/electrolyte double layer capacitance behavior. Thus, the bulk resistance R_b of the separators can be acquired from the high-frequency intercept of the Nyquist plot on the Z' axis (shown in inset curve of Fig. 5). It is seen that the bulk resistance of NFs/PET/NFs separator (3.17 Ω) is slight lower than PP separator (3.56 Ω). Accordingly, the ion conductivity of the NFs/PET/NFs separator is calculated to be 0.55 mS cm^{-1} by Equation (3), surpasses that of the commercial PP separator (0.28 mS cm^{-1}). This relatively high ion conductivity of the NFs/PET/NFs separator is due to the high electrolyte wettability and three-dimensional hierarchical nano-porous structure [21–25]. These results suggest that the ion conductivity of the NFs/PET/NFs separator can well meet the conductivity requirement of lithium-ion battery applications.

3.5. Performance of the NF separator assembled cell

3.5.1. Galvanostatic charge/discharge

The galvanostatic charge/discharge performance of the separators is investigated shown in Fig. 6. It can be seen that the discharge capacity at 0.2 C of the NFs/PET/NFs separator is about 152 mA g^{-1}, which is higher than that of the commercial PP separator (140 mA g^{-1}). The columbic efficiency of the NFs/PET/NFs separator is measured to be 98.7% comparable to that of the PP separator (98.5%). It is noticed that the difference between the charge and discharge voltages of the NFs/PET/NFs separator is 0.15 V, which is smaller than that of the commercial PP Separator (0.18 V). The difference between the charge and discharge voltages referred to IR drop is the loss in voltage due to resistance (ohmic) polarization in lithium-ion batteries. Polarization results from ohmic resistance of Li^+ ion conducting through the electrolyte-saturated separator, electronic conductivity between the anode (Li metal) and cathode ($LiFePO_4$), and contacting resistance between the electrode and current collector [11,25–28]. Since ohmic polarization is profoundly influenced by the Li^+ ions movement in the separator, the IR drop is closely associated with the ionic conductivity for different separators. The Li^+ ion conductivity is a function of separator's porosity, electrolyte affinity, pore size, thickness and so on. In present study, due to the affinity of electrolyte and high porous structure, a relatively higher Li^+ ionic conductivity (0.55 mS cm^{-1}) in our NFs/PET/NFs separator than that in the PP commercial separator (0.28 mS cm^{-1}) is achieved. Higher ionic conductivity leads to smaller degree of ohmic polarization in lithium-ion battery, thus resulting in smaller voltage loss for battery with NFs/PET/NFs separator than that with PP separator.

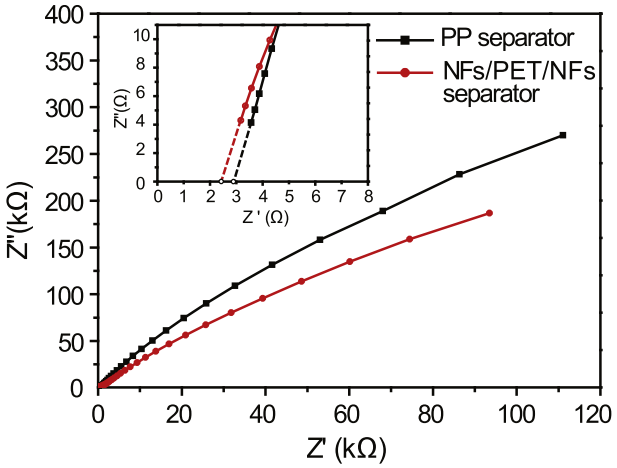

Fig. 5. Nyquist plot of PP and NFs/PET/NFs separators at open-circuit potential with an AC voltage of a perturbation signal 5 mV.

3.5.2. Rate capability

The cell performance of the commercial PP separator and the NFs/PET/NFs separator at various discharge conditions (0.2 C, 0.5 C,

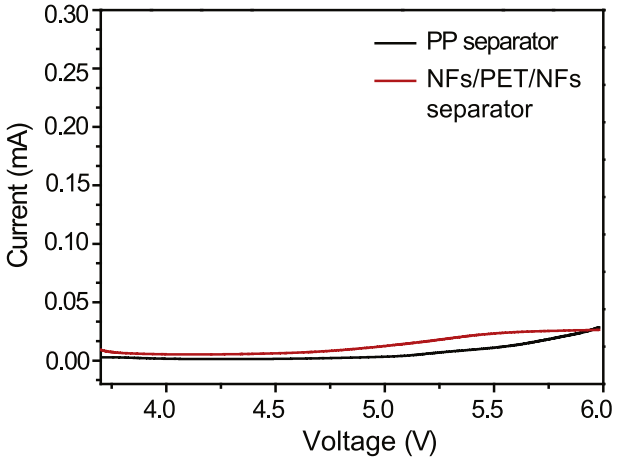

Fig. 4. Linear sweep voltammetry curves for the electrolyte-saturated PP and NFs/PET/NFs separators at a scan rate 1.0 mV s^{-1}.

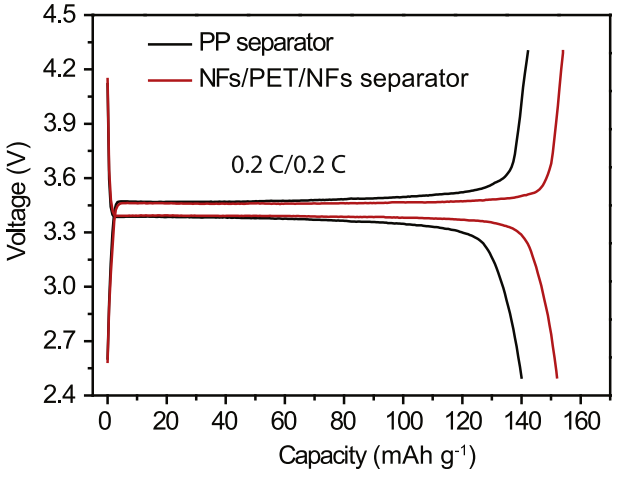

Fig. 6. The galvanostatic charge/discharge behaviors of PP and NFs/PET/NFs separators 0.2 C/0.2 C charge/discharge current density.

1 C, 2 C) are shown in Fig. 7(a) and (b). The discharge voltage as well as discharge capacity of the cells gradually decrease at higher discharge current density. As seen in Fig. 7(b), no unstable or abnormal discharge curves occur for NFs/PET/NFs separator. Fig. 7(c) summarizes the discharge capacities of the commercial PP and the NFs/PET/NFs separators. The NFs/PET/NFs separator always shows higher discharge capacities than those of PP separator at various discharge current densities ranging from 0.2 C to 2 C. Moreover, the difference in the discharge capacities between the PP and NFs/PET/NFs separator becomes more pronounced at higher discharge current densities. Though a separator does not influence the theoretical electrical energy storage (upper limit of the cell capacity) or output, its physical properties greatly influence the practical performance and safety of the battery. Considerable

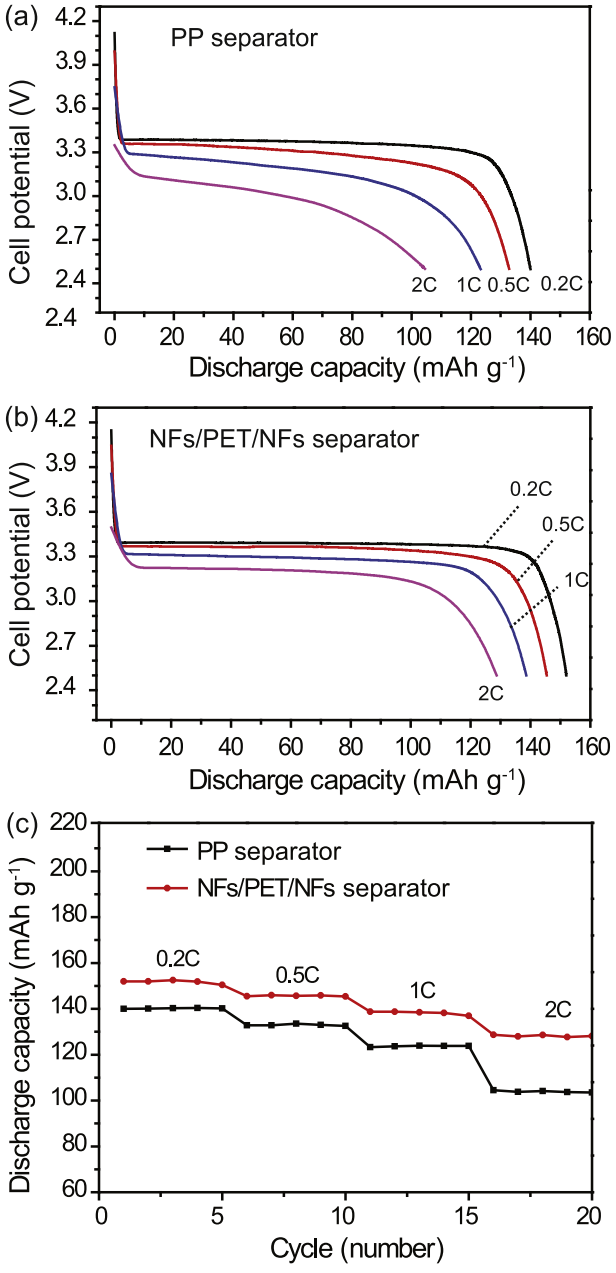

Fig. 7. The discharge voltage profiles of cells at different discharge current density with the separator (a) PP, (b) NFs/PET/NFs and (c) summary of C-rate capability of the cells with the two separators.

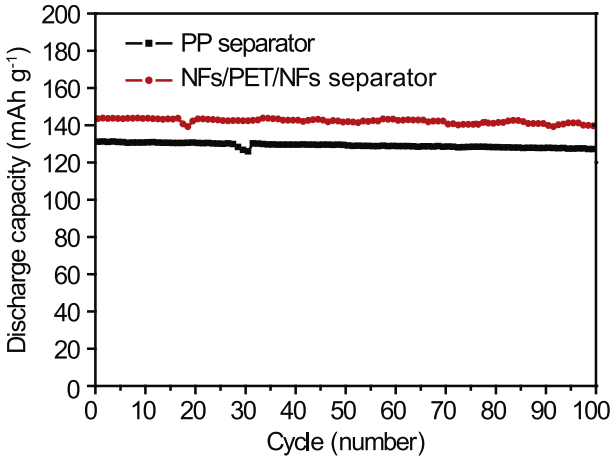

Fig. 8. Cycling performance of the cells with the PP and NFs/PET/NFs separators at a constant current charge/discharge condition 0.5 C/0.5 C.

literature have suggested that the rate capability of lithium-ion batteries and safety can be significantly influenced by the ion conductivity of electrolyte-saturated separator due to ohmic polarization especially at higher discharge current density [8,25–28]. As reported above, the NFs/PET/NFs separator possesses hierarchical nanoscaled porous structure and superior electrolyte wettability, thus resulting in higher ion conductivity than that of the commercial PP separator and a corresponding improved C-rate discharge capability at different current densities. Since the ohmic polarization at higher discharge current densities is more pronounced for separators, as a consequence, the difference in the discharge capacities between the PP and NFs/PET/NFs separator is becoming larger.

3.5.3. Cycle performance

Fig. 8 shows the cycling performance of the $LiFePO_4$/Li half cells using the NFs/PET/NFs and the commercial PP separators at a charge/discharge current density of 0.5 C/0.5 C. The NFs/PET/NFs separator always shows higher discharge capacity than that of PP separator during cycles. After 100 cycles, the retention of discharge capacity for NFs/PET/NFs separator is about 97.4%, while that for PP separator is about 97%. This excellent cycling performance could be ascribed to the well-designed hierarchically nanoporous structure and good electrolyte wettability, which facilitate the ion transport and electrolyte retention during cycling [29–32].

4. Conclusion

In this study, a novel hierarchically structured and highly hydrophilic NFs/PET/NFs separator composed of a PET nonwoven sandwiched between two interconnected PVA-*co*-PE nanofibrous membranes is successfully developed for lithium-ion battery. The notable feature of this NFs/PET/NFs separator is an electrolyte-philic, highly porous and hierarchically nanoscaled structure. Due to its inherent structural advantage, the NFs/PET/NFs separator shows superior electrolyte wettability, lower thermal shrinkage, and higher ion conductivity, in comparison to the PP separator. These structural characteristics enable the NFs/PET/NFs separator to provide an ideal cell performance including outstanding C-rate capability, high capacity and excellent cycling performance. This indicates that the NFs/PET/NFs separator is a promising material for practical application in lithium-ion battery due to it low cost production and high performance.

Acknowledgment

The authors thank the National Natural Science Foundation of China (51273152) for financial support.

Appendix A. Supplementary data

Supplementary data related to this article can be found at http://dx.doi.org/10.1016/j.jpowsour.2014.04.151.

References

[1] H. Li, Z. Wang, L. Chen, X. Huang, Adv. Mater. 21 (2009) 4593–4607.
[2] J. Hassoun, S. Panero, P. Reale, B. Scrosati, Adv. Mater. 21 (2009) 4807–4810.
[3] M.R. Palacin, Chem. Soc. Rev. 38 (2009) 2565–2575.
[4] L. Ji, O. Toprakci, M. Alcoutlabi, Y. Yao, Y. Li, S. Zhang, B. Guo, Z. Lin, X. Zhang, ACS Appl. Mater. Interfaces 4 (2012) 2672–2679.
[5] M.V. Reddy, G.V. Subba Rao, B.V. Chowdari, Chem. Rev. 113 (2013) 5364–5457.
[6] G. Venugopal, J. Moore, J. Howard, S. Pendalwar, J. Power Sources 77 (1999) 34–41.
[7] C. Yang, Z. Jia, Z. Guan, L. Wang, J. Power Sources 189 (2009) 716–720.
[8] P. Arora, Z. Zhang, Chem. Rev. 104 (2004) 4419–4462.
[9] C.M. Costa, M.M. Silva, S. Lanceros-Méndez, RSC Adv. 3 (2013) 11404–11417.
[10] S.S. Zhang, J. Power Sources 164 (2007) 351–364.
[11] J.-R. Lee, J.-H. Won, J.H. Kim, K.J. Kim, S.-Y. Lee, J. Power Sources 216 (2012) 42–47.
[12] J.-K. Kim, G. Cheruvally, X. Li, J.-H. Ahn, K.-W. Kim, H.-J. Ahn, J. Power Sources 178 (2008) 815–820.
[13] D. Wang, W. Xu, G. Sun, B.S. Chiou, ACS Appl. Mater. Interfaces 3 (2011) 2838–2844.
[14] J. Zhang, Z. Liu, Q. Kong, C. Zhang, S. Pang, L. Yue, X. Wang, J. Yao, G. Cui, ACS Appl. Mater. Interfaces 5 (2013) 128–134.
[15] H. Xiang, J. Chen, Z. Li, H. Wang, J. Power Sources 196 (2011) 8651–8655.
[16] F. Zhang, X. Ma, C. Cao, J. Li, Y. Zhu, J. Power Sources 251 (2014) 423–431.
[17] J. Song, M.-H. Ryou, B. Son, J.-N. Lee, D.J. Lee, Y.M. Lee, J.W. Choi, J.-K. Park, Electrochim. Acta 85 (2012) 524–530.
[18] T.-H. Cho, M. Tanaka, H. Ohnishi, Y. Kondo, M. Yoshikazu, T. Nakamura, T. Sakai, J. Power Sources 195 (2010) 4272–4277.
[19] C. Cao, L. Tan, W. Liu, J. Ma, L. Li, J. Power Sources 248 (2014) 224–229.
[20] M. Kim, Y.S. Kim, Y.-G. Lee, J.H. Park, RSC Adv. 3 (2013) 16708–16713.
[21] Y. Zhu, F. Wang, L. Liu, S. Xiao, Z. Chang, Y. Wu, Energy Environ. Sci. 6 (2013) 618–624.
[22] J. Lee, C.-L. Lee, K. Park, I.-D. Kim, J. Power Sources 248 (2014) 1211–1217.
[23] Y. Liang, S. Cheng, J. Zhao, C. Zhang, S. Sun, N. Zhou, Y. Qiu, X. Zhang, J. Power Sources 240 (2013) 204–211.
[24] M. Rao, X. Geng, Y. Liao, S. Hu, W. Li, J. Membr. Sci. 399–400 (2012) 37–42.
[25] J.-J. Woo, Z. Zhang, N.L. Dietz Rago, W. Lu, K. Amine, J. Mater. Chem. A (2013) 8538–8540.
[26] Y. Zhu, S. Xiao, Y. Shi, Y. Yang, Y. Wu, J. Mater. Chem. A (2013) 7790–7797.
[27] S. Xiao, F. Wang, Y. Yang, Z. Chang, Y. Wu, RSC Adv. 4 (2014) 76–81.
[28] J.-R. Lee, J.-H. Won, S.-Y. Lee, J. Electrochem. Sci. Technol. 2 (2011) 51–56.
[29] H.-S. Jeong, E.-S. Choi, J.H. Kim, S.-Y. Lee, Electrochim. Acta 56 (2011) 5201–5204.
[30] S.-J. Chun, E.-S. Choi, E.-H. Lee, J.H. Kim, S.-Y. Lee, S.-Y. Lee, J. Mater. Chem. 22 (2012) 16618–16626.
[31] J.-H. Cho, J.-H. Park, J.H. Kim, S.-Y. Lee, J. Mater. Chem. 21 (2011) 8192–8198.
[32] H.-S. Jeong, E.-S. Choi, S.-Y. Lee, Electrochim. Acta 86 (2012) 317–322.